SOBENA

25th National Congress on Maritime Transportation, Ship and Offshore Construction

Rio de Janeiro, 10th to 12th November 2014

Two-dimensional Numerical Simulation of an Oscillating Cylinder in Turbulent Flow: Comparison to Experimental Results

Marcelo Caire
Pedro Henrique Affonso Nòbrega
Rachel Viana Khalil
Instituto SINTEF do Brasil (ISdB)
Department of Marine Technology

Abstract:

Fatigue life assessment of risers and pipelines are mostly based, for engineering purposes, on semi-empirical methods that combines structural models with hydrodynamic coefficients obtained from experiments for specific conditions. They might be different from those observed in operation and performing experiments for each particular condition is economically unattractive. Consequently, there is a need for the development of numerical methodologies that are able to take into account conditions closer to those encountered in operation (e.g. near seabed effects for free span pipelines). As the computational cost of full 3D CFD simulations remains high, our goal is to evaluate the feasibility of using 2D RANS simulations to obtain the desired hydrodynamic coefficients. Turbulence models are expected to significantly influence the results, as from Re > 300 the wake of the cylinder is turbulent and the flow exhibits three-dimensional features. In this work, 2D simulations of the flow around a smooth circular cylinder are performed for a Reynolds number of 10000 using the RNG $k-\varepsilon$ turbulence model for two configurations: i) stationary cylinder and ii) forced cross-flow oscillations. The obtained drag and lift coefficients are compared to available experimental data.

Keywords: *circular cylinder, turbulent flow, cross-flow, vortex induced vibrations*

1 – INTRODUCTION

Free spanning pipelines is an increase concern for the oil and gas industry as deepwater fields can be developed in areas with very irregular seabed conditions. The developed spans may also change location and size from time to time increasing the uncertainties associated to pipeline integrity conditions.

The incidence of ocean currents, may lead to separated flow and vortex shedding. As a consequence, the pressure distribution around the pipeline will experience a periodic change in the horizontal and vertical directions, namely the cross-flow (CF) and in-line (IL) components. The resultant time varying stresses may significantly affect the accumulation of fatigue damage, which is one of the main concerns for the pipe integrity.

This phenomenon is known as vortex induced vibrations (VIV), and a number of variables may affect its response, such as: a) surface roughness, b) incoming turbulence, c) shear flow, d) flow behavior change due to proximity with the seabed, e) dynamic interaction between adjacent free spans, f) damping due to pipe soil interaction, g) interaction between CF and IL response, among others.

The assessment of fatigue in risers and pipelines for engineering purposes still strongly relies on semi-empirical methods combining hydrodynamic coefficients obtained experimentally and structural models. For instance, the software VIVANA (2014) used for

the prediction of VIV in slender structures, couples a non-linear finite-element model with a set of experimental hydrodynamic data. These data sets provide hydrodynamic coefficients such as drag, lift and added mass for a circular cylinder. The coefficients are presented as a function of the non-dimensional oscillation frequency $f_0 D/V$ and the amplitude ratio A_0/D. Here, f_0 is the cylinder oscillation frequency, D is the cylinder diameter, V is the free flow velocity and A_0 is the amplitude of the oscillations.

Gopalkrishan (1993) has obtained this set of data by subjecting a smooth circular cylinder to forced oscillations at a Reynolds number of 10000. Figure 1 shows the contour plot of the mean drag coefficient as an example.

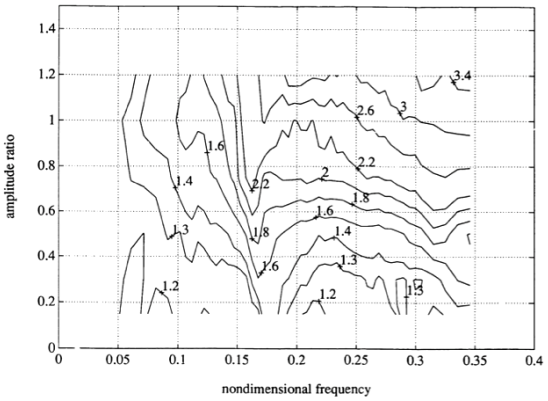

Figure 1 – Mean drag coefficient of an oscillating cylinder as a function of oscillation frequency and amplitude for Re = 10000 (Gopalkrishnan, 1993).

Gopalkrishnan's experimental coefficients have been obtained for specific conditions, which may be different from those observed in the operation of offshore structures (e.g. diverse Re numbers, rough cylinder due to marine growth or corrosion, seabed boundary layer effect, etc). Performing experiments for each particular condition is undesirable and thus, there is a need for assessment methodologies that are able to take into account conditions closer to those encountered in operations.

The increase in computational capabilities has encouraged the use of CFD in this direction. However, the computational cost of 3D simulations considering fluid-structure interaction over the whole structures remains prohibitive for engineering purposes at high Reynolds numbers. Gustafsson (2012) has performed such full 3D simulations for a Reynolds number of 1.5 x 10^5. The high cost associated with this kind of computation comes not only from the need of solving both structural and fluid equations, but also from the turbulence models.

As an alternative approach, CFD could be used to reproduce the hydrodynamic coefficients data set used as input for semi-empirical methods. In particular, the use of 2D numerical simulations could avoid unaffordable costs from an engineering project perspective and help reducing some analysis uncertainties.

Numerical simulations of the turbulent flow around circular cylinders, for a variety of Reynolds numbers, have been performed by previous authors. Dong and Karniadakis (2005) have used direct numerical simulation (DNS) to reproduce the turbulent flow around a circular cylinder, either fixed or oscillating at Re = 10000 and the results showed a very good agreement with Gopalkrishnan's results for a moderate amplitude ratio of $A_0/D = 0.3$. However, the cost of 3D DNS simulations remains prohibitively high for engineering purposes. More recently, Nguyen and Temarel (2014) evaluated the use of 2D RANS simulations, using different turbulent models, for the same conditions as Dong and Karniadakis (2005). For the standard $k-\omega$ model, the drag coefficient showed good agreement with measurements but the lift coefficient was not well captured at the low frequency range. For the realizable $k-\varepsilon$ model employed in their study, the opposite has been observed, where the drag coefficient has not presented a good agreement but the lift followed the experimental trend.

In the present paper, 2D Reynolds-Averaged Navier-Stokes (RANS) numerical simulations are carried out using the RNG $k-\varepsilon$ turbulence model for two configurations: i) stationary cylinder, to validate the modeling methodology and ii) forced cross-flow oscillations, to compare the numerical results with the available experimental data obtained from Gopalkrishnan's experiment. The numerical experiments are carried out for a Reynolds number of 10.000, an oscillation amplitude of $A_0 = 0.3D$ and non-dimensional frequencies ranging from $0.05 \leq f_o D/V \leq 0.35$.

2 – NUMERICAL MODEL

2.1 – Problem description

Vortex shedding from a smooth circular cylinder is a function of the non-dimensional Reynolds number, defined as,

$$\mathrm{Re} = \frac{\rho V D}{\mu} \qquad (1)$$

where ρ is the fluid density and μ the dynamic viscosity. A schematic figure of the flow near separation is presented in Fig. 2. As described by Summer and Fredsoe (2006), for Re > 5 the boundary layer over the cylinder surface will separate due to adverse pressure gradient when the kinetic energy of the fluid particles is not high enough to overcome the downstream pressure field.

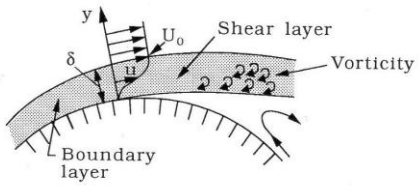

Figure 2 – Shear layer. (Summer and Fredsoe, 2006)

Near Re = 40, the pair of vortices generated by the boundary layer separation becomes unstable, leading to the phenomenon called vortex shedding. The vortex shedding frequency f_s is proportional to the incoming flow velocity and cylinder diameter, and can be described as,

$$S_t = \frac{f_s D}{V} \tag{2}$$

where S_t is called the Strouhal number. After Re = 300, the flow becomes turbulent in the cylinder wake but remains laminar in the boundary layer. This is the regime found for the Reynolds number adopted in this work: 10000.

There are two contributions to the resultant force on the cylinder due to the turbulent flow: one from the pressure and the other from the friction. The relative contribution from the friction to the total mean drag force, for example, is a function of the Re number, and is usually around 2-3% as described by Achenbach (1968). The total mean in-line force is the sum of these two forces, and can be described as follows,

$$\bar{F}_D = \tfrac{1}{2}\rho D V^2 \int_0^{2\pi} \left[\left(\frac{\bar{p} - p_0}{\rho V^2} \right) \cos(\theta) + \left(\frac{\bar{\tau}_0}{\rho V^2} \right) \sin(\theta) \right] d\theta \tag{3}$$

in which $\bar{p}$ is the pressure and $\bar{\tau}_0$ is the shear stress on the cylinder surface, and the over bar denotes time averaging. Due to the vortex shedding, the *stationary cylinder* experiences an oscillating lift force F_{L0} at f_s frequency, a mean drag force $\bar{F}_D$ and an oscillating drag force F_{D0} at twice the shedding frequency. For an *oscillating cylinder* subjected to sinusoidal oscillations, additional frequency components may compete with the Strouhal frequency. As described by Gopalkrishnan (1993), depending on the amplitude A_0 and period of the forced oscillation $T_0 = 1/f_0$, the response may be in the *lock-in regime*, where the cylinder motion dominates the response and the Strouhal frequency component is irrelevant.

Considering the two frequency components, the lift and drag forces can be written, respectively, as,

$$F_L = F_{L0} \sin\left(\frac{2\pi}{T_0} t + \phi_{L0} \right) + F_{Ls} \sin\left(\frac{2\pi}{T_s} t + \phi_{Ls} \right) \tag{4}$$

$$F_D = \bar{F}_D + F_{D0} \sin\left(2\frac{2\pi}{T_0} t + \phi_{D0} \right) + F_{Ds} \sin\left(2\frac{2\pi}{T_s} t + \phi_{Ds} \right) \tag{5}$$

where the subscript s is related to the shedding frequency f_s and 0 is associated to the forced oscillation frequency f_0. The lift and drag coefficients may be obtained by dividing equations (4) and (5) by $\tfrac{1}{2}\rho D V^2$, leading to,

$$C_L = C_{L0} \sin\left(\frac{2\pi}{T_0} t + \phi_{L0} \right) + C_{Ls} \sin\left(\frac{2\pi}{T_s} t + \phi_{Ls} \right) \tag{6}$$

$$C_D = \bar{C}_D + C_{D0} \sin\left(2\frac{2\pi}{T_0} t + \phi_{D0} \right) + C_{Ds} \sin\left(2\frac{2\pi}{T_s} t + \phi_{Ds} \right) \tag{7}$$

The coefficients presented in Eq. (6) and (7) may be obtained from the lift and drag force time series through Fourier coefficient analyses, as will be presented in section 3.

2.2 – Governing Equations

The incompressible fluid dynamic analysis is performed in ABAQUS/CFD (2013). Its solver uses the integral form of the conservation equations. For an arbitrary volume, the unsteady momentum equations can be written as,

$$\begin{aligned}&\frac{d}{dt}\int_{\Omega}\rho\,\mathbf{v}\,d\Omega+\int_{V}\rho\,\mathbf{v}\otimes\left(\mathbf{v}-\mathbf{v}_{m}\right).\mathbf{n}dS\\&=-\int_{\Omega}\nabla p\,d\Omega+\int_{S}\boldsymbol{\tau}.\mathbf{n}\,dS+\int_{\Omega}f\,d\Omega\end{aligned}\tag{8}$$

where Ω is an arbitrary control volume with surface area S, $\mathbf{n}$ is the outward normal to S, ρ is the fluid density, p is the pressure, $\mathbf{v}$ is the velocity vector, $\boldsymbol{\tau}$ is the viscous shear stress and $\mathbf{v}_m$ is the velocity of the moving mesh when the arbitrary Lagrangian-Eulerian (ALE) methodology is employed. The viscous stress $\boldsymbol{\tau}$ is also referred to as the deviatoric stress $\mathbf{S}$, given by,

$$\mathbf{S}=\mu\dot{\boldsymbol{\gamma}}\tag{9}$$

being $\dot{\boldsymbol{\gamma}}$ the engineering shear strain rate.

2.3 – Numerical method: resolution of the Navier-Stokes equations

A transient incompressible turbulent flow analysis with automatic time incrementation based on a fixed Courant-Freidrichs-Lewy (CFL = 0.45) condition is used in the present work. For the time-dependent problem, a second-order projection method is used for an arbitrary deforming domain where a node-centered finite-element discretization is adopted for the pressure and a cell-centered finite volume discretization for all the other transported variables (such as velocity, temperature, turbulence, etc.). According to Abaqus documentation, this hybrid approach guarantees accurate solutions and eliminates the possibility of spurious pressure modes (without the need for any artificial dissipation) while retaining the local conservation properties associated with traditional finite volume methods.

For the oscillating cylinder, the modeling of turbulent flow requires invoking the arbitrary Lagrangian-Eulerian (ALE) methodology within Abaqus/CFD, where the mesh is deformed to accommodate the boundary displacements. The mesh deformation incurs additional solution costs associated with frequent updating of wall-normal distances for the turbulent flow problem.

2.2 – Turbulence model

There is no single universal turbulence model that can adequately handle all possible flow conditions and geometrical configurations.

In a recent work of Nguyen and Temarel (2014), for example, they have investigated the influence of the following models on the 2D flow around a stationary cylinder at Re=10000: standard $k-\varepsilon$ (SKE), realizable $k-\varepsilon$ (RKE), standard $k-\omega$ (SKW) and SST $k-\omega$. They concluded that both RKE and SKW can be employed to predict the response, with an indication that SKW might work better for higher Reynolds numbers. When it comes to the oscillating cylinder, the RKE presented a good agreement for the lift coefficient magnitude but not a very good correlation with the drag coefficient. The opposite is verified for the SKW model.

In the present case study, the RNG $k-\varepsilon$ turbulence model is adopted. It involves an equation for the turbulent kinetic energy, *k*, and the energy dissipation rate, ε, where the RNG version of the model computes the coefficients using the Renormalization Group Theory. The model equations are,

$$\begin{aligned}&\frac{d}{dt}\int_{\Omega}\rho\,k\,d\Omega+\int_{S}\rho\,k\left(\mathbf{v}-\mathbf{v}_{m}\right).\mathbf{n}\,dS\\&=\int_{S}\left(\mu+\frac{\mu_{T}}{\sigma_{k}}\right)\nabla k.\mathbf{n}\,dS\\&+\int_{\Omega}\tau_{ij}S_{ij}\,d\Omega-\int_{\Omega}\rho\,\varepsilon\,d\Omega\end{aligned}\tag{10}$$

$$\begin{aligned}&\frac{d}{dt}\int_{\Omega}\rho\,\varepsilon\,d\Omega+\int_{S}\rho\,\varepsilon\left(\mathbf{v}-\mathbf{v}_{m}\right).\mathbf{n}\,dS\\&=\int_{S}\left(\mu+\frac{\mu_{T}}{\sigma_{\varepsilon}}\right)\nabla\varepsilon.\mathbf{n}\,dS\\&+\int_{\Omega}C_{\varepsilon1}\frac{\varepsilon}{k}\tau_{ij}S_{ij}\,d\Omega-\int_{\Omega}\rho\,C_{\varepsilon2}\frac{\varepsilon^{2}}{k}d\Omega\end{aligned}\tag{11}$$

where the turbulent viscosity is given by,

$$\mu_{T}=\frac{\rho\,C_{\mu}k^{2}}{\varepsilon}\tag{12}$$

and C_{μ}, σ_k and σ_{ε} are model constants. The turbulence kinetic energy can be expressed as,

$$k = \frac{3}{2}\left(V\, I_u\right)^2 \tag{13}$$

and I_u is the turbulence intensity, defined by,

$$I_u = \frac{\sqrt{\overline{v'^2}}}{\overline{v}} \tag{14}$$

being $\overline{v'^2}$ the root-mean square value of the velocity fluctuation and $\overline{v}$ the mean value of velocity. It has been shown by Cheung and Melbourne (1983) that the St variation with Re is highly dependent on the level of turbulence in the approaching flow, as the boundary layer separation comes earlier with higher turbulence intensity. For Re < 10^5 the influence seems to decrease.

The main difference between the standard $k-\varepsilon$ and the RNG $k-\varepsilon$ models lies in the additional term in the dissipation equation, which gives the following coefficient,

$$C_{\varepsilon 2} = \tilde{C}_{\varepsilon 2} + \frac{C_\mu \eta^3 (1-\eta/\eta_0)}{1+\beta\eta^3} \tag{15}$$

where $\tilde{C}_{\varepsilon 2}$ and β are model coefficients and η is described by,

$$\eta = \frac{k}{\varepsilon}\sqrt{2 S_{ij} S_{ij}} \tag{16}$$

In regions of large strain rate, $\eta > \eta_0$, the RNG model yields a lower turbulent viscosity than the standard $k-\varepsilon$, being, consequently, more responsive to the effects of rapid strain rate. More details can be found in Yakhot *et al.* (1992).

2.4 – Geometry, mesh and boundary conditions

The computational model dimensions have been chosen such that the inlet, outlet and far field boundaries are far enough from cylinder's surface to decrease boundary effects.

The diameter, D, of the cylinder is 1 m. The inlet is placed 4 diameters away from cylinder's center while the outlet is 12 diameters away. The far-field boundaries are each placed 4 diameters away from the cylinder center. Figure 3 shows the main model dimensions.

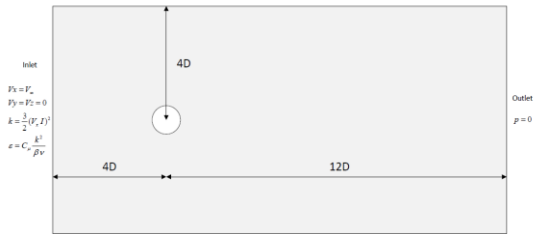

Figure 3 – Model dimensions

The properties of the fluid are chosen to achieve a flow Reynolds number of 10000 based on cylinder's diameter and the inlet velocity. The fluid density is chosen to be $\rho = 1000 kg/m^3$ and the viscosity is $\mu = 0.001 Pa.\sec$. The fluid is assumed to be quiescent and hence, the initial velocity is zero everywhere.

An inlet velocity of $V_x = 0.01 m/s$ is considered. An outlet boundary condition is specified with the fluid pressure set to zero, $p = 0$. The far-field velocity is assumed to be equal to the inlet velocity. The velocity normal to the symmetry planes (V_z) is assumed to be zero to constrain the out-of-plane flow. A turbulent intensity of 1% and a viscosity ratio $\nu_t / \nu = 1$ were also applied at the inlet, which correspond to a weak turbulence condition.

The model consists of 32000 hexahedral fluid elements (FC3D8) with one-element in the through-thickness direction. The mesh is refined in a zone of $0.5D$ around the cylinder with the intention of adequately capturing the flow behavior near the cylinder wall and the boundary layer. This zone is divided in 100 elements along the axial direction with a bias of 14, which leads to the height of the element closest to the wall y_p being 0.001*D*. The circumference is equally divided in 200 elements. Figure 4 a zoom near the cylinder surface.

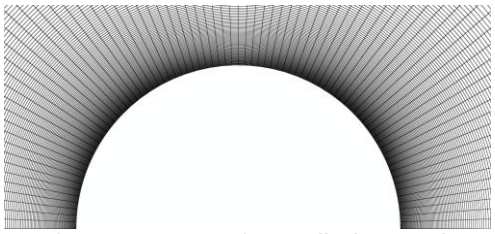

Figure 4 – Zoom into cylinder mesh

For the oscillating cylinder, a no-slip/no-penetration wall boundary condition requires that the fluid velocity at the wall remain equal to the cylinder's velocity. The following time-dependent mesh displacement is prescribed using an amplitude definition,

$$Y_x = A_0 \sin\left(\frac{2\pi t}{T_0}\right) \quad (17)$$

Since the cylinder wall displacement has been prescribed, the fluid velocity is also known and defined as,

$$V_x = \frac{2\pi A_0}{T_0}\cos\left(\frac{2\pi t}{T_0}\right) \quad (18)$$

For the present case study, we employ constant amplitude of $A_0 = 0.3D$ and a range of T_0 to cover the non-dimensional frequencies $0.05 \leq f_o D/V \leq 0.35$, where $f_0 = 1/T_0$. This is the same range as observed in the experimental results presented by Gopalkrishan (1993).

3 – RESULTS AND DISCUSSION

3.1 – Turbulent flow across an stationary circular cylinder: Re=10.000

The mean drag coefficient $\bar{C}_D$, the root mean square of the lift coefficient C'_{L0} and the Strouhal number S_t are shown below in Table 1 for different numerical models (2-equation turbulence models and DNS), for the experimental data available and for the empirical functions proposed by Norberg (2003), as follows,

$$S_t = 0.1853 + 0.0261 \times \exp\left[-0.9\log\left(\frac{\mathrm{Re}}{1600}\right)^{2.3}\right] \quad (19)$$

$$C'_{L0} = 0.52 - 0.06\left[\log\left(\frac{\mathrm{Re}}{1600}\right)\right]^{-2.6} \quad (20)$$

Table 1 – Results for the fixed cylinder case

	Mean drag	*Lift RMS*	*Strouhal*
RNG k-e	1.180	0.432	0.2487
RKE (Nguyen and Temarel (2014))	0.920	0.400	0.2100
SKW (Nguyen and Temarel (2014))	1.250	0.700	0.2000
DNS (Dong & Kariadakis (2005))	1.143	0.317	0.2030
Norberg (2003)	-	0.411	0.2006
Gopalkrishnan (1993)	1.186	0.271	0.1932

The present model shows very good agreement for drag coefficient when compared to both experimental data and DNS. The lift coefficient also presents a very good agreement with Norberg empirical function, although the Strouhal number is somewhat higher than the average results.

3.2 – Turbulent flow across an oscillating circular cylinder: Re=10.000

The mean drag coefficient $\bar{C}_D$ against non-dimensional frequency is shown in Fig. 5. For the experimental data it can be observed that a sharp amplification peak occurs at $f / f_0 \approx 0.17$ which is slightly below the Strouhal frequency. A second amplification peak is observed near a frequency of 0.3. The numerical results present a very good correlation, although the peak close to the Strouhal frequency is somewhat delayed and not as high.

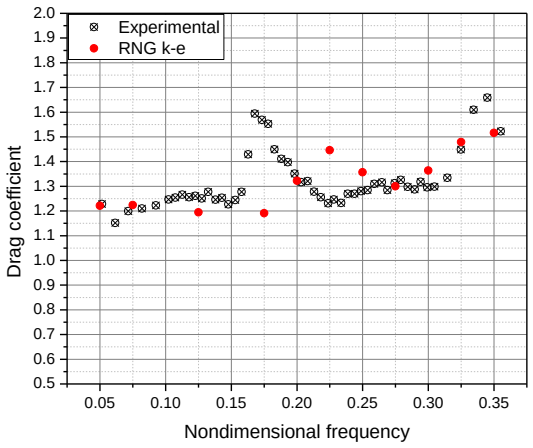

Figure 5 – Drag coefficient x non-dimensional frequency

For the lift force time series results, a discrete Fourier transform analysis is performed. The amplitude response is shown for three selected forced oscillation periods (T_0=2000, 500 and 285.71 s) in Fig. 6, 7 and 8 respectively. It's important to point out that, in the experimental data presented by Gopalkrishnan (1993), the oscillations corresponding to the vortex shedding frequency are neglected. As can be observed from Fig. 6, for example, that is not the case for high forced oscillations frequencies where the dominant amplitude component is not associated to f_0. Figure 7 is an example of the lock-in region, where forced oscillation frequency dominates

the response and there is only one peak. In Fig. 8, although the amplitude at $f / f_0 \approx 1$ dominates the response, there is also a component present at a lower frequency.

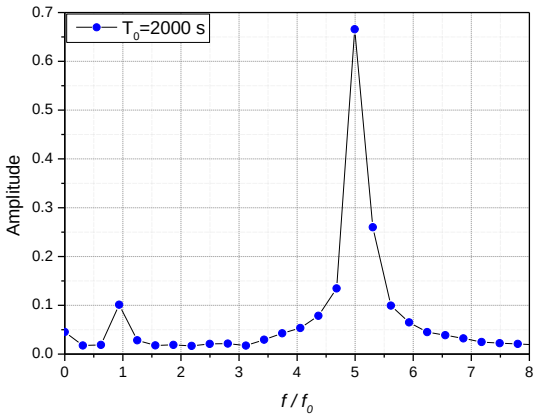

Figure 6 – Amplitude x non-dimensional frequency of the lift coefficient for T_0=2000 s

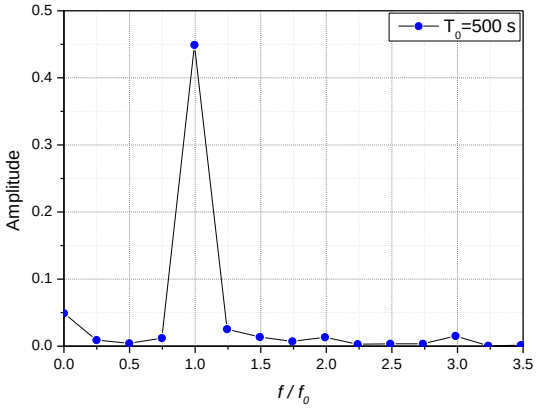

Figure 7 – Amplitude x non-dimensional frequency of the lift coefficient for T_0=500 s

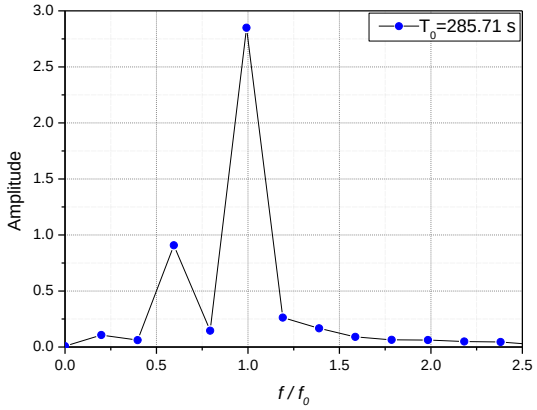

Figure 8 – Amplitude x non-dimensional frequency of the lift coefficient for T_0=285.71 s

In order to compare the numerical results with the experimental data available, only the component associated with the oscillation frequency ($f / f_0 \approx 1$) is presented in Fig. 9, which correspond to the coefficient C_{L0} from Eq. (6).

A good correlation is obtained for frequencies below the lock-in region, where very small values can be observed. The general trend is also captured (although it presents a delay), where there is an abrupt increase of the coefficient when the oscillation frequency is close to the shedding frequency. As opposed to the experimental results, the numerical simulation seems to follow a gradual increase of the lift coefficient for non-dimensional frequencies higher than $f / f_0 \succ 0.3$.

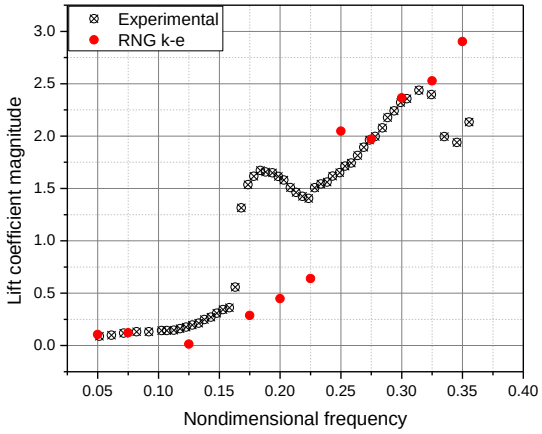

Figure 9 – Lift coefficient magnitude x non-dimensional frequency

4 – SUMMARY AND CONCLUSIONS

In the present paper, 2D Reynolds-Averaged Navier-Stokes (RANS) numerical simulations are carried out for two configurations: i) stationary cylinder, to validate the modeling methodology and ii) forced cross-flow oscillations, to compare the numerical results with the available experimental data obtained from Gopalkrishnan's experiment. The numerical experiments were carried out for a Reynolds number of 10.000, an oscillation amplitude of $A_0 = 0.3D$ and non-dimensional frequencies ranging from $0.05 \leq f_o D/V \leq 0.35$.

Although the Strouhal number was higher than the experimental results, both in the stationary and forced oscillation cases, a very good overall agreement with the drag and lift coefficients was obtained using the RNG $k-\varepsilon$ turbulence model.

In order to effectively evaluate the applicability of CFD analysis for estimation of hydrodynamic coefficients employed in semi-

empirical models, the whole range of oscillations amplitudes and non-dimensional frequencies currently adopted in the semi-empirical codes have to be numerically calculated and used as input data. This may allow the comparison of the uncertainties associated to the calculation of pipeline fatigue lifetime, for example.

Acknowledgments

The authors would like to acknowledge Instituto SINTEF do Brasil (ISdB) for the present work development.

5 – REFERENCES

[1] ACHENBACH, E. Distribution of local pressure and skin friction around a circular cylinder in cross-flow up to $Re=5x10^5$. *Journal of Fluid Mechanics*, Volume 34, Number 4, pages 625-639, 1968.

[2] ABAQUS v6.13, Program documentation, 2013.

[3] CHEUNG, J.C.K, MELBOURNE, W.H., Turbulence effects on some aerodynamic parameters of a circular cylinder at supercritical Reynolds numbers. *Journal of Wind Engineering and Industrial Aerodynamics*, Volume 14, pages 399-410.

[4] GOPALKRISHNAN, R. *Vortex-induced Forces on Oscillating Bluff Cylinders.* D. Sc. Thesis, Department of Ocean Engineering, MIT, Boston, 1993.

[5] DONG, S., & KARNIADAKIS, G. E. (2005). DNS of low past a stationary and oscillating cylinder at. Journal of Fluids and Structures, 20(4), 519–531.

[6] GUSTAFSSON, A. *Analysis of Vortex-Induced Vibrations of Risers*. MSc thesis, Chalmers University of Technology, Sweden, 2012

[7] NGUYEN, L.T.T., TEMAREL, P., Numerical simulation of an oscillating cylinder in cross-flow at a Re number of 10.000: forced and free oscillations, OMAE2014-23394, *33rd International Conference on Ocean, Offshore and Arctic Engineering*, San Francisco, California, USA, 2014.

[8] NORBERG, C., Fluctuating lift on a circular cylinder: review and new measurements. *Journal of Fluids and Structures*, Number 17, pages 57-96, 2003.

[9] SUMER, B.M, FREDSOE, J., Hydrodynamics around cylindrical structures, revised edition, 2006.

[10] VIVANA, Program Documentation, 2014

[11] YAKHOT, V., THANGAM, S., GATSKI, T.B., ORSZAG, S.A., SPEZIALE, C.G., Development of turbulence models for shear flows by a double extension technique. *Physics of Fluids A*, Volume 4, Number 7, pages 1510-1520, 1992.